Structural Impact of Heparin Binding to Full-Length Tau As Studied by NMR Spectroscopy†

Nathalie Sibille,‡ Alain Sillen,‡ Arnaud Leroy,‡,§ Jean-Michel Wieruszeski,‡ Barbara Mulloy,‖ Isabelle Landrieu,‡ and Guy Lippens*,‡

CNRS UMR 8576, Unité de Glycobiologie Structurale et Fonctionnelle, Université des Sciences et Technologies de Lille 1, 59655, Villeneuve d'Ascq Cedex, France, Laboratoire de biochimie appliquée, Faculté de Pharmacie (Paris XI), 5 rue Jean-Baptiste Clément, 92296 Chatenay-Malabry Cedex, France, and Laboratory of Molecular Structure, National Institute for Biological Standards and Control, Blanche Lane, South Mimms, Potters Bar, Herts EN63QG, U.K.

Received May 16, 2006; Revised Manuscript Received August 11, 2006

ABSTRACT: The neuronal Tau protein is involved in stabilizing microtubules but is also the major component of the paired helical filaments (PHFs), the intracellular aggregates that characterize Alzheimer's disease (AD) in neurons. *In vitro*, Tau can be induced to form AD-like aggregates by adding polyanions such as heparin. While previous studies have identified the microtubule binding repeats (MTBRs) as the major player in Tau aggregation, the fact that the full-length protein does not aggregate by itself indicates the presence of inhibitory factors. Charge and conformational changes are of uttermost importance near the second (R2) and third (R3) MTBR that are thought to be involved directly in the nucleation of the aggregation. Recently, the positively charged regions flanking the MTBR were proposed to inhibit PHF assembly, where hyperphosphorylation neutralizes these basic inhibitory domains, enabling Tau−Tau interactions. Here we present results of an NMR study on the interaction between intact full-length Tau and small heparin fragments of well-defined size, under conditions where no aggregation occurs. Our findings reveal (i) micromolar affinity of heparin to residues in R2 and R3, (ii) two zones of strong interaction within the positively charged inhibitory regions flanking the MTBR, and (iii) another interaction site upstream of the two inserts encoded by exons 2 and 3. Three-dimensional heteronuclear NMR experiments demonstrate that the interaction with heparin induces β-strand structure in several regions of Tau that might act as nucleation sites for its aggregation but indicate as well α-helical structure in regions outside the core of PHF. In the PHF, the residues outside of the core maintain sufficient mobility for NMR detection and recover their unbound chemical shift values after an overnight incubation at 37 °C with heparin. Heparin thus becomes integrated into the rigid core region of the PHF, probably providing the charge compensation for the lysine-rich stretches that form upon the in-register, parallel stacking of the repeat regions.

Implicated in microtubule stabilization, the Tau protein appears in the neuron in six different isoforms (for a review, see ref *1*). The discovery that this protein aggregates in brain affected by Alzheimer's disease (AD)[1] (*2*, *3*) has attracted substantial research efforts, especially since the clinical symptoms of cognitive decline correlate well with the occurrence of Tau aggregates (*4*). Electron microscopy reveals that Tau aggregates in the form of paired helical filaments (PHFs) or straight filaments (SFs), and subsequent clumping of these filaments can lead to the characteristic tangles observed in the brain.

Rather little is known about the structure of Tau in either its free, microtubule-bound, or aggregated state. At the level of the primary sequence, several regions have been identified, for instance, the N-terminal projection domain, the proline-rich region, and the microtubule binding repeat domain (MTBR) that features up to four internal sequence repeat motifs (R1−R4) and is framed by positively charged inhibitory domains that appear to prevent Tau aggregation. The longest mature isoform (Tau441, 441 residues) differs from the shortest fetal one (Tau352, 352 residues) by the presence of the second repeat sequence (R2) within the MTBR and of two inserts in the N-terminal region (*1*). Small

† The NMR facility used in this study was funded by the Région Nord-Pas de Calais (France), the CNRS, the Universities of Lille 1 and Lille 2, and the Institut Pasteur de Lille. N.S. was funded by an AIRMA Grant (Association Internationale pour la Recherche sur la Maladie d'Alzheimer) and A.S. by a European Training and Mobility Grant (HPRN-CT-2002-00241).

* To whom correspondence should be addressed. Tel: (33) 3 20 33 72 41. Fax: (33) 3 20 43 69 49. E-mail: Guy.Lippens@univ-lille1.fr.

‡ Université des Sciences et Technologies de Lille 1.

§ Laboratoire de biochimie appliquée.

‖ National Institute for Biological Standards and Control.

[1] Abbreviations: AD, Alzheimer's disease; CD, circular dichroism; HMW, high molecular weight heparin; HSQC, heteronuclear single-quantum coherence; IR, infrared spectroscopy; LMW, low molecular weight heparin; MTBR, microtubule binding repeat; NMR, nuclear magnetic resonance; NOESY, nuclear Overhauser effect spectroscopy; PHF, paired helical filament; R1−4, repeats constituting the MTBR [R1 (residues 244−273), R2 (residues 274−304), R3 (residues 305−335), and R4 (residues 336−367)]; RDC, residual dipolar coupling; SAXS, small angle X-ray scattering; SF, straight filament; ThS, thioflavin S; TOCSY, total correlation spectroscopy.

10.1021/bi060964o CCC: $33.50
Published on Web 09/20/2006

angle X-ray scattering (SAXS) and other spectroscopic techniques, such as circular dichroism (CD) and infrared spectroscopy (IR), indicate that the isolated protein in solution is a random coil or Gaussian polymer (*5*, *6*). These techniques, however, only give an averaged view of the overall structure, and local elements of secondary and/or tertiary structure might well have escaped observation. Only very recently, on the basis of a limited number of FRET pairs, a global hairpin model of Tau has been proposed, with the C-terminal end of Tau folding (at least transiently) over into the vicinity of the microtubule-binding repeat domain (*7*). NMR spectroscopy can detect residual local structure on a per-residue basis, but the large size of Tau and its highly degenerate amino acid composition present a serious obstacle. Recent solution NMR studies, however, have been undertaken to reveal elements of residual structure in both the isolated MTBR region (*8*, *9*) and in full-length Tau (*10*, *11*).

Phosphorylation of Tau is an important regulatory mechanism for its function under both physiological and pathological conditions. It leads to the detachment of the protein from the microtubules (*1*, *12*), and aggregated Tau is always found in a hyperphosphorylated state (*13*). Incubation with heparin *in vitro* at 37 °C can cause aggregation of even unphosphorylated Tau (*14*, *15*). The 16 kDa heparin (HMW) is typically employed to induce Tau filament formation after prolonged incubation at 37 °C, but working at low temperature (20 °C) allows to keep Tau in its soluble form and amenable to observation by solution-state NMR. Furthermore, smaller heparin fragments (4.2 kDa) do not induce aggregation of the full-length Tau while still interacting with Tau and therefore allow the mapping in greater detail of the interaction zones. The molecular basis for this process remains unknown, although the discovery that other polyanions such as RNA (*16*) or arachidonic acid (*17*) can also cause formation of filaments indicates that Tau aggregation is rather influenced by electrostatics than by the precise nature of the negatively charged polymer.

We report here a thorough characterization of the interaction between heparin and full-length Tau and find that both α-helical and extended β structure elements can be induced, depending on the location in the primary sequence. Importantly, the extended β structure propensity is mostly enforced in the R2 and R3 repeats, believed to be nuclei of the aggregation process through the presence of the PHF6* and PH6 peptides, respectively (*18*), whereas α-helix is induced in stretches that resemble more the canonical lysine-rich binding motifs of heparin (*19*). Interaction of heparin with the proline-rich region just preceding the MTBR, and symmetrically in the region just following the MTBR, brings the necessary charge neutralization and possible conformational changes of those regions that prevent full-length Tau aggregation. Finally, the observation that the residues of Tau that are not integrated into the PHF core recover their chemical shift values after an overnight incubation with heparin at 37 °C and the absence of NMR signals of heparin after the aggregation process is completed not only suggest that the polyanion is integrated into the rigid core of the PHF but equally that heparin contributes to the charge compensation for the lysine-rich stretches that appear upon the in-register, parallel stacking of the repeat regions within the PHF core.

MATERIALS AND METHODS

Sample Preparation. Heparin. Samples were from the commercially available heparin, with a mean molecular mass around 16 kDa (Sigma-Aldrich, Saint-Quentin Fallavier, France), or a smaller 4.2 kDa fragment, an almost monodisperse tetradecasaccharide prepared as described previously (*20*). Briefly, a sample of bovine lung heparin was partially depolymerized by digestion with heparinase I (donated by Leo Pharmaceutical Products, Ballerup, Denmark). The resulting oligosaccharides were separated by preparative gel permeation chromatography on Bio-Gel P10 (Bio-Rad) and characterized using analytical high-performance gel permeation chromatography (HPLC) (*21*). As with most commercially available heparins, all samples used in this study were composed of more than 70% trisulfated disaccharide repeat units.

[U-^{15}N]-Labeled Tau441 Sample. Recombinant Tau441 (441 residues, Met_1-Leu_{441}) was expressed and purified as described previously (*10*).

Specifically [U-^{13}C,Lys-^{15}N]-Labeled Tau441 Sample. Lysine-specific ^{15}N labeling of otherwise ^{13}C-labeled Tau was obtained by adding ^{15}N-labeled lysine to uniformly ^{13}C-labeled M9 medium. Induction delays were limited to 2 h in order to minimize isotopic scrambling. Purification was identical to that of the uniformly labeled samples.

Alignment Media. Samples typically contained 20 μM [U-^{15}N]- or [U-^{13}C,Lys-^{15}N]-labeled Tau in either free or complexed form in both isotropic and anisotropic conditions. For the latter, inert alignment media must be used to prevent potential binding of the fully unstructured protein. Thus, both free and LMW heparin-bound Tau was aligned by adding a 5% (w/v) mixture of polyoxyethylene 5-lauryl ether ($C_{12}E_5$) and 1-hexanol (Sigma) with a molar ratio of $C_{12}E_5$/1-hexanol = 0.85 (*22*). A quadrupolar splitting of the solvent deuterium resonance of ca. 30 Hz for the two samples confirmed the efficiency of the alignment. The latter ratio hence allowed alignment at the same temperature (20 °C) where assignments had been obtained (*10*).

Fluorescence Spectroscopy. Steady-state fluorescence was monitored on a PTI fluorescence spectrometer (PTI, Lawrenceville, NJ). The excitation and emission slit widths were set to 2 and 4 nm, respectively, whereas the polarizer was set to the magic angle. To monitor the filament formation, an excitation wavelength of 440 nm was used, whereas the emission spectrum was scanned from 450 to 600 nm. Thioflavin S (Sigma-Aldrich) concentration in all samples was 0.02 mg/mL. Tau (8 μM) in an aqueous buffer containing 25 mM sodium phosphate, 25 mM NaCl, 300 μM DTT (pH 6.9), and ThS was incubated with 0.8 μM 16 kDa heparin (HMW) or with varying amounts of the 4.2 kDa heparin (LMW) at 37 °C. The fluorescence was monitored for 15 h.

Electron Microscopy. After incubation, the original sample was diluted 100 times, and a drop was then placed on a formvar/carbon coated grid for 1 min. After drying, the grid was stained with 2% uranyl acetate for 1 min. Transmission electron microscopy was performed on a Hitachi 7500-2, Japan electron microscope operated at 80 kV.

CD Spectroscopy. For the CD measurements, we used stock solutions of Tau (at 20 μM) and heparin (at 200 μM) in a 25 mM NaCl and 25 mM sodium phosphate buffer

adjusted to pH 6.9 (buffer A) to prepare the different samples in a final volume of 500 μL. Tau protein concentration was adjusted in all the samples to 1 μM based on a molar absorption coefficient of 7400 $M^{-1}\cdot cm^{-1}$ at 200 nm (*23*). The blank solution (without Tau) contained the same amount of heparin as in the measured samples, in buffer A. The signal from the blank scan was subtracted from the corresponding sample scan. The contribution of heparin to the signal was negligible. CD spectra were obtained on a Model CD6 spectrometer (Jobin-Yvon-Spex, Longjumeau, France) at 20 °C in order to avoid any aggregation during the scanning, using a quartz sample cell with 1 mm path length. The ellipticity was scanned from 190 to 250 nm with an increment of 0.5 nm, an integration time of 2 s, and a constant band-pass of 2 nm. The specific ellipticity of Tau was calculated assuming a mean residue weight of 104.

NMR Spectroscopy. NMR samples typically were prepared in 25 mM Tris-d_{11} buffer at pH 6.8, 50 mM NaCl, 2.5 mM EDTA, 5 mM DTT, 1 mM TMSP-d_4 (trimethylsilyl propionate), and 5% D_2O. All NMR spectra were recorded at 20 °C on a Bruker DMX600 spectrometer equipped with a triple resonance cryogenic probehead (Bruker, Karlsruhe, Germany).

Measurement on [U-^{15}N]-Labeled Tau441 Sample. For the titration experiments, 80 μM free [U-^{15}N]-labeled Tau was added to appropriate amounts of lyophilized heparin (4.2 kDa) to obtain molar ratios of heparin:Tau = 0.25, 0.5, 1, 3, and 5. ^{1}H−^{15}N heteronuclear correlation spectra (^{15}N-HSQC) were acquired using sensitivity-enhanced pulse sequences (*24*) and coherence selection by gradients. NMR spectra were recorded with 64 scans per increment and 128 complex points in the ^{15}N dimension. The 3D NOESY-^{15}N-HSQC spectra were acquired at 800 MHz with a regular triple resonance probe head with [152, 64, 2048] complex points in the [F_1 = ^{1}H, F_2 = ^{15}N, F_3 = ^{1}H] dimensions. One-bond N−H RDCs ($^1D_{NH}$) were determined from 2D ^{15}N-HSQC IPAP spectra (*29*) with a ^{15}N FID resolution of 3.9 Hz/point.

Measurements on Specifically [U-^{13}C,Lys-^{15}N]-Labeled Tau441. The initial sample concentration was 190 μM. Titration with the smaller 4.2 kDa heparin fragment was performed on a 160 μM Tau sample by adding increasing amounts of LMW heparin lyophilized aliquots to obtain molar ratios of heparin:Tau = 1.125, 2.25, and 4.5. Chemical shifts were extracted from 3D CBCA[CO]NH (*25*) and HNCO (*26*) spectra acquired with FID resolutions of 4.1 Hz (F_3 = H^N), 21.7 Hz (F_1 = ^{15}N), 75 Hz (F_2 = CACB), and 72.1 Hz (F_2 = CO). $^3J_{HNH\alpha}$ couplings were derived from a 3D HNHA experiment (*27*) with analogous FID resolutions in F_3 = H^N, and F_1 = ^{15}N, and 47.1 Hz in F_2 = HNHA. A mixing time of 300 ms was used for the 3D NOESY-^{15}N-HSQC spectra (*28*), using the same acquisition parameters as for the 3D HNHA. One-bond N−H RDCs ($^1D_{NH}$) were determined in the same manner as on the U-^{15}N sample.

Data Processing. Spectra were processed using Bruker TOPSPIN 1.3. 3D spectra were processed with 2048 points in the ^{1}H dimension and a 45° shifted sine bell window function and 512 complex points in both indirect dimensions with a cosine bell window function and forward linear prediction of the same number of complex points recorded. 2D spectra were processed with 4096 complex points in the ^{1}H dimension and 1024 complex points in the ^{15}N dimension.

Data Analysis. The 2D spectra were analyzed using the software SNARF (van Hoesel FHJ, 2000 SNARF v.0.8.9, University of Groningen, The Netherlands). Secondary ^{13}C and $^1H_\alpha$ chemical shift were used as indicators for residual local secondary structure (*30*, *31*), taking into account deviations from random coil shifts occurring in unfolded or unstructured proteins due to the local sequence (*32*). $^3J_{HNH\alpha}$ couplings were derived from intensity ratios of H_NH_α cross-peaks (S_{cross}) and corresponding H_NH_N diagonal peaks (S_{diag}) using the equation:

$$^3J_{HNH\alpha} = \frac{\arctan\sqrt{-(S_{cross}/S_{diag})}}{2\pi\zeta f}$$

where 2ζ, the total evolution time for the homonuclear $^3J_{HNH\alpha}$ coupling, was set to 26.1 ms. The empirical scaling factor f, required to correct for differential T_1 relaxation effects (*27*), can be set to 1 since the apparent selective T_1 of the H_α spin is long enough for the highly flexible Tau that behaves like a protein with a correlation time of approximately 4 ns, as estimated from the T_1/T_2 ratio (*33*). Couplings measured have an error estimated to ca. 0.3 Hz.

For the interaction studies, the variation of both ^{1}H and ^{15}N chemical shifts was calculated as follows:

$$\Delta\delta = \sqrt{(\Delta\delta_H)^2 + 0.2(\Delta\delta_N)^2}$$

Dissociation constants were deduced by nonlinear least-squares fitting of the observed chemical shift changes ($\Delta\delta$) to the molar ratio (X) of heparin to Tau concentration [Tau] using the quadratic function (*34*):

$$\Delta\delta = \frac{\Delta\delta_{max}}{2}\left\{1 + X + \frac{K_D}{[Tau]} - \sqrt{\left(1 + X + \frac{K_D}{[Tau]}\right)^2 - 4X}\right\}$$

$^1D_{NH}$ values were calculated as the difference between (apparent) coupling values measured in anisotropic and isotropic solutions, respectively, and then inverted to account for the negative gyromagnetic ratio of ^{15}N.

RESULTS

(1) Molecular Characterization of the Interacting Partners. We have previously reported a partial assignment for the Tau protein, based on the assumed validity of random coil shifts and on a novel "peptide mapping by NMR" strategy (*11*). Yet, many of the Tau resonances in the HSQC spectrum overlap considerably, thereby hindering a precise mapping of the interaction with heparin. Since we expected electrostatics to dominate the interaction between the positively charged Lys and Arg side chains of Tau and the negative charges on the heparin polymer, we produced a [^{15}N-Lys/U-^{13}C]-labeled sample by growing the transformed bacteria in a minimal culture medium with $^{14}NH_4Cl$ and ^{13}C-glucose as the only sources of nitrogen and carbon, while adding directly the ^{15}N-Lys as a free amino acid. Introducing such residue-specific ^{15}N labeling into an otherwise uniformly [U-^{13}C]-labeled protein allows to record triple resonance correlation experiments and, thus, establish sequential connectivities. 3D CBCA(CO)NH and HNCO spectra on the

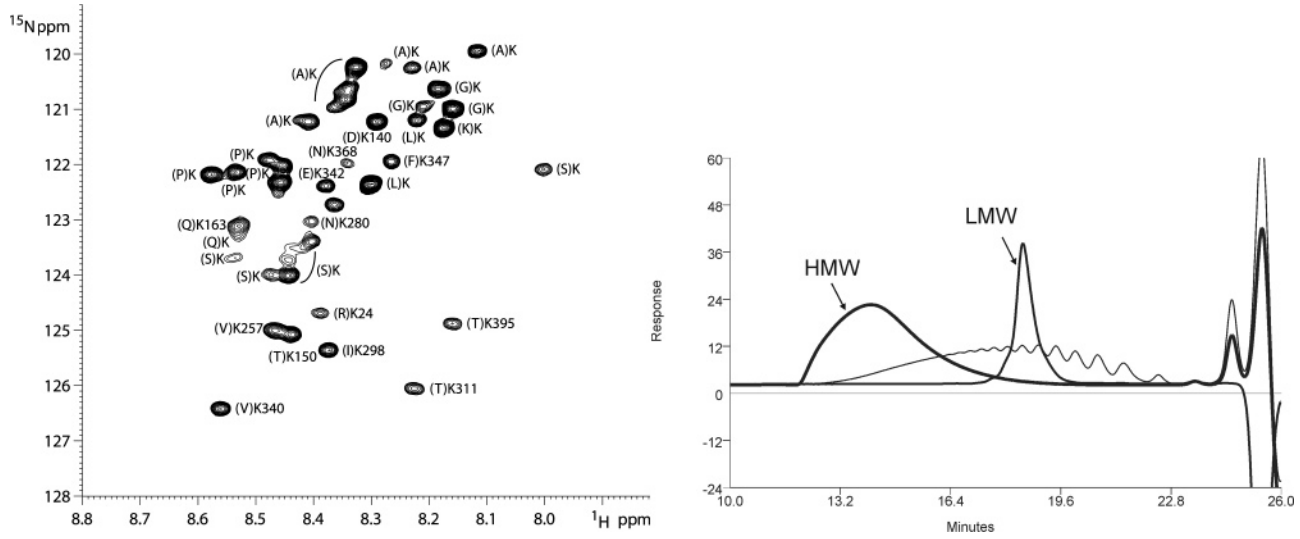

FIGURE 1: (Left) Annotated ^{15}N-HSQC of the specifically [U-^{13}C,Lys-^{15}N]-labeled Tau sample. (Right) Analytical high-performance gel permeation chromatography of high molecular weight heparin (HMW) and low molecular weight heparin (LMW) as defined in the text, with a chromatogram (thin line) of a calibrant material (second IRR LMW heparin for MW calibration, NIBSC 90/686). Partially resolved peaks in the calibrant arise from even-numbered oligosaccharides; the retention time of LMW corresponds to the tetradecasaccharide.

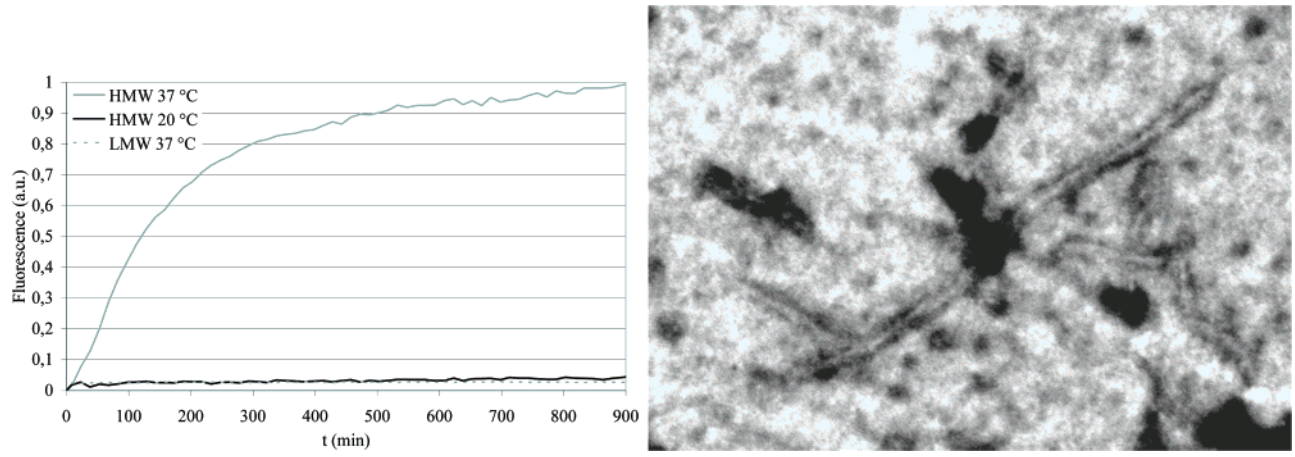

FIGURE 2: (Left) ThS fluorescence during the incubation of 8 μM Tau with 4 μM LMW heparin at 37 °C (dotted gray curve) and 0.8 μM HMW heparin at 37 °C (gray curve) and 20 °C (black curve). (Right) Electron microscopy of full-length Tau after incubation with HMW heparin at 37 °C.

[U-^{13}C, Lys-^{15}N]-labeled Tau sample provided spectral information on the 44 [Xaa-^{13}C]-[Lys-^{15}N] residue pairs. The C_β, C_α, and CO chemical shifts of the Xaa residues preceding lysine along with the general validity of random coil shifts for the highly flexible Tau protein then allowed their attribution to distinct amino acids. By matching these Xaa-Lys pairs to the Tau primary sequence, we could assign 13 of the 44 resolved lysine signals unambiguously (Figure 1, left), whereas we previously had assigned only two of them.

Heparin is a linear polysaccharide, and most preparations are both heterogeneous in sequence and polydisperse due to variations in chain length. Commercial heparin preparations, however, consist predominantly of a trisulfated disaccharide repeat unit, with other sequences forming only a minor proportion. The molecular mass range extends from about 3 to 35 kDa, with an average mass of 16 kDa (high molecular weight sample, HMW) (*35*). This polydispersity is problematic in that a true molar concentration is difficult to calculate, and in that it may hide molecular weight dependence of any property measured. We therefore used as a second interacting partner, an almost monodisperse heparin fragment that was characterized as a tetradecasaccharide (Figure 1, right), with a well-defined molecular mass of 4.2 kDa (low molecular weight sample, LMW). Importantly, there is almost no molecular weight overlap between HMW and LMW. Accordingly, this fragment does not lead to Tau aggregation into PHF (see below) and thereby simplifies considerably the interaction study by NMR spectroscopy.

(2) Macroscopic Characterization of the Molecular Interaction. Incubating the Tau sample with a substoichiometric (1:10) amount of HMW heparin during 16 h at 37 °C produced *bona fide* PHF, as indicated by thioflavin S (ThS) fluorescence and electron microscopy (*36*) (Figure 2). Incubation of the same mixture at 20 °C, however, did not lead to an increase in ThS fluorescence (*37*) during 16 h (Figure 2), indicating that no fibril formation occurs within the duration of a typical NMR experiment (1−12 h). We also used the smaller LMW heparin fragment with a much more uniform size distribution. When incubating Tau with the latter at 37 °C, no increase in ThS fluorescence was detected, regardless of the ratio of LMW heparin to Tau, and electron microscopy likewise revealed the absence of

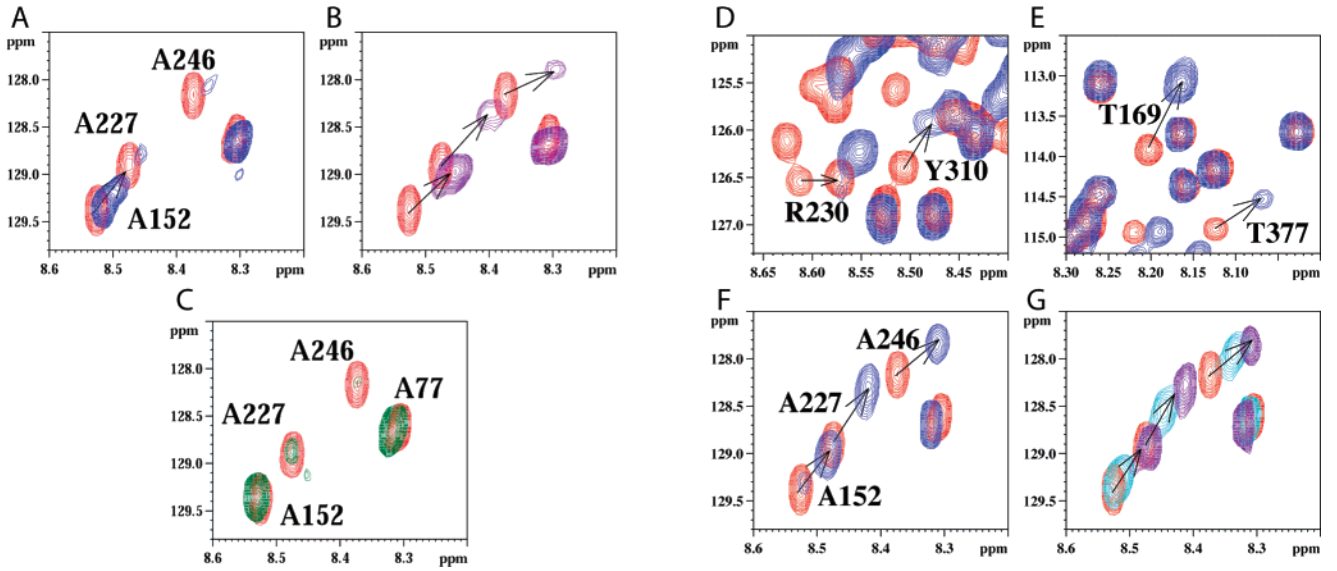

FIGURE 3: (A−C) $^{1}H-^{15}N$ HSQC spectra of Tau without (red) or with HMW heparin with a 0.1:1 (A, blue) or 2:1 (B, purple) ratio. (C, green) Same sample as (A) after overnight incubation at 37 °C. This sample mainly contains PHF-Tau. (D−F) Selected zooms of the $^{1}H-^{15}N$ HSQC spectra of isolated ^{15}N-labeled Tau (red) or of Tau with a 1:1 ratio of the 4.2 kDa heparin fragment (blue). (G) Titration experiment with LMW heparin in a 0.5:1 (light blue) or 3:1 (purple) ratio.

any fibrils. Figure 2 shows a representative ThS fluorescence curve for the LMW fragment at a ratio of 1:2 to Tau, which contains roughly the same amount of heparin subunits as the 1:10 HMW heparin:Tau sample. As previously reported for the heparin−gelsolin interaction (*38*), the size of the heparin fragment therefore seems to play an important role in inducing Tau aggregation.

(3) Per-Residue Characterization of the Heparin−Tau Interaction. Without aggregation at 20 °C on the time scale of the NMR experiments, the ^{15}N-HSQC spectra of the HMW heparin:Tau mixture exclusively monitors the interaction without concurring PHF formation. In agreement with a previous study on the interaction between a very short heparin fragment (3 kDa) and a fragment of Tau (*9*), we observed significant chemical shift differences for residues within the MTBR, but in our experimental system with the full-length Tau, we equally observed pronounced chemical shift differences for residues outside the MTBR. The binding kinetics, however, proved to be unfavorable for NMR observation, causing severe line broadening of the Tau signals even at low HMW heparin concentrations (1:10 heparin:Tau) (Figure 3A). This line broadening was also observed for samples saturated with the HMW heparin (e.g., 2:1 heparin:Tau) (Figure 3B). After incubating this 1:10 HMW heparin:Tau sample overnight at 37 °C, we could reproduce our previously reported ^{15}N-HSQC intensity pattern for the *bona fide* PHF (*36*), where intensities decrease monotonically roughly from residue 100 toward the fibril core. Remarkably, though, we lose all chemical shift variations that HMW heparin induces in soluble Tau (see, for example, Ala152 in Figure 3C). This suggests that all heparin is sequestered within the rigid PHF core and thereby loses its capacity to reversibly associate with parts of Tau outside of the core, as happens when the protein is still in its soluble state. To confirm this assumption, we attempted to directly monitor the anomeric heparin protons during the aggregation process. The fibers were assembled in a D_2O buffer to avoid masking of the anomeric signals by the residual water signal. Yet, we could not detect any anomeric proton resonances after Tau polymerization, although they were clearly visible as a cluster downfield of the residual water signal for isolated heparin in D_2O buffer (*35*). This confirms that when Tau aggregated into PHFs, no free heparin is left to interact with its flexible regions. The polyanion therefore is an integral part of the core region, although we do not know how it is structurally integrated.

(4) Mapping the Heparin−Tau Interaction Using a Short Heparin Fragment (LMW). We performed titrations on a [U-^{15}N]- and [^{15}N -Lys]-labeled Tau sample by adding increasing amounts of LMW heparin. The observed chemical shift changes (Figure 3) are largely the same as those induced by HMW heparin, confirming the validity of the LMW fragment for mapping the heparin−Tau interaction. Yet, binding of LMW heparin caused significantly less line broadening, most probably due to faster exchange kinetics. Moreover, the gradual shift of signals during the titration experiment allowed us to plot chemical shift changes as a function of the LMW heparin:Tau ratio (Figure 4). While the presence of multiple interaction sites precluded a rigorous evaluation of the resulting dissociation constants, applying the general one site/one ligand model to our titration curves nevertheless yields apparent K_D values that allow a relative ranking of heparin affinity to different regions of full-length Tau (Figure 4, sequence with coloring).

[U-^{15}N]-Labeled Tau441 Titration. Although signal overlap prevented the determination of accurate dissociation constants for many signals in this uniformly labeled sample, we were able to rank the strength of interaction for several other residues in the full-length Tau (Figure 4, sequence with color coding). Most Tau signals affected by the interaction with heparin are in the fast exchange limit, as indicated by their gradual frequency shift with increasing heparin concentration. For a few cross-peaks, however, exchange is in the slow exchange limit, with two cross-peaks coexisting simultaneously for the free and bound form. An example is Ala152, where we observe a gradual decrease of the signal intensity at the initial position, concomitant with a gradual appearance of a new peak next to it (Figure 3F). We

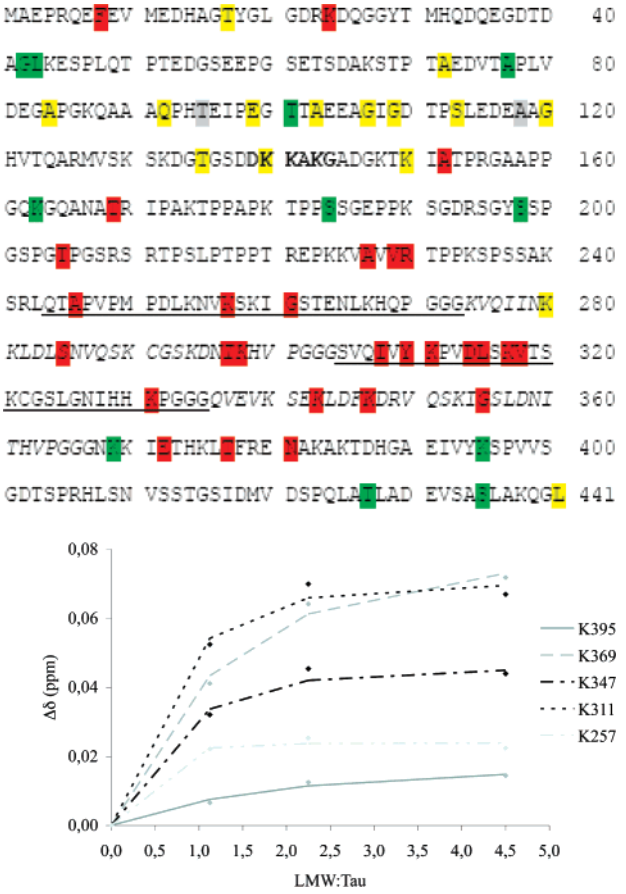

FIGURE 4: (Top) Primary sequence of Tau with color coding according to the affinity measured for the short heparin fragment: red, K_D values in the 10 μM range; green, K_D values in the 100 μM range; yellow, K_D in the midmillimolar range; gray, peak shifts but overlap prevents K_D determination. In bold is the consensus sequence for heparin binding, where we can deduce the strongest binding based on the slow exchange for Ala152. The MTBRs are indicated as underlined or italic sequences. (Bottom) Specifically [U-^{13}C,Lys-^{15}N]-labeled Tau titration curves with LMW heparin indicating K_D values of the order of 100 μM for Lys395 (C-ter), Lys369 (R4), and Lys347 (R4) while stronger interaction for Lys311 (R3) and specifically Lys257 (R1).

discovered another site of strong interaction in the region following the fourth repeat (R4 residues 336−370) and a remarkable cluster in the proline-rich region just preceding the MTBR (Figure 4, sequence with color coding). The titration curves of several peaks inside the MTBR region define a cluster of strong interaction in the second (R2 residues 274−304) and third repeat (R3 residues 305−335). Micromolar K_D values were derived for Tyr310 and Ser316, suggesting that the PHF6 peptide (V_{306}QIVYK$_{311}$) within R3 contains an important binding site for the short heparin fragment. Ser285 displayed a similar K_D value, suggesting that the very homologous PHF6* fragment (V_{275}QIINK$_{280}$) likewise binds strongly to heparin. If these short peptides are truly acting as nucleators for the PHF formation, we expect their charge state to be important for their aggregation behavior (*39*, *40*). Net charge will directly be influenced by the interaction with the negatively charged heparin, suggesting one possible role for the polyanion-induced PHF formation.

Specifically [U-^{13}C,Lys-^{15}N]-Labeled Tau441 Titration. For most of the 44 lysines, we observed shifts of the amide group

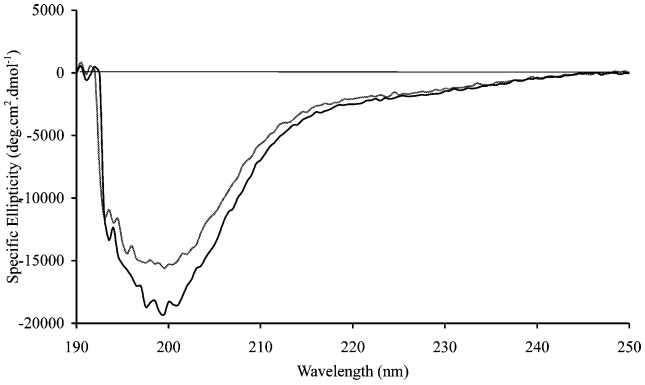

FIGURE 5: CD spectra of isolated Tau (dark curve) or Tau with an equimolar amount of HMW heparin (light curve).

signal upon heparin addition, confirming that electrostatic attraction between the negatively charged heparin and the basic lysine residues of Tau plays a key role in the interaction. The reduced signal overlap allowed us to fit most of the titration curves to a one ligand/one binding site model and hence derive individual dissociation constants (K_D) for many lysine residues in the specifically Lys-^{15}N-labeled sample. The obtained values were not completely uniform, with a K_D in the order of 10 μM for Lys24 (following a basic Arg23) and only in the range of 100 μM for Lys140 (preceding Lys141), probably due to the presence of two acidic residues (Asp) at positions 138 and 139. Micromolar dissociation constants were found for Lys257 within R1 (residues 244−273), which corresponds to one of the tightest interacting regions. In the absence of negatively charged residues, and combined with Lys254 and Lys259, this stretch clearly approaches the canonical heparin binding site (*19*). In R2, we confirmed the strong binding site for heparin with a K_D in the 10 μM range for Lys298. The strong interaction determined for R3 using the uniformly labeled sample (Figure 4) was confirmed by similar 10 μM range K_D values for Lys311 within the PHF6 core and for Lys330 (Figure 4). The identical IVYK$_{395}$ motif located in R4 interacts 10-fold less strongly (with K_D values of the order of 100 μM for Lys395), probably because the preceding residues, Glu391 and Gln307, respectively, differ, with the former bringing in a negative charge. Within R4, we obtained 10 μM K_D values for Lys343 and Lys347 and a 100 μM value for Lys369 (Figure 4). In summary, these data confirm that electrostatics drive the interaction between heparin and Tau, with stronger binding where the basic lysine/arginine residues cluster along the primary sequence, whereas negatively charged residues weaken the interaction.

(5) Structural Consequences of the Heparin−Tau Interaction. Overall Changes in Secondary Structure. We first tested by circular dichroism (CD) whether the interaction of Tau with heparin induces secondary structure changes. The CD spectrum of Tau resembles that of a random coil polymer, with a broad minimum at 195−200 nm. Addition of an equimolar amount of the long 16 kDa heparin fragment leads to small but significant spectral changes, with a less pronounced minimum at 200 nm suggesting a reduced random coil contribution (Figure 5). Because both CD spectra were acquired on samples with identical Tau concentrations (see Materials and Methods), a simple dilution effect can be excluded as the origin of the spectral differences. More

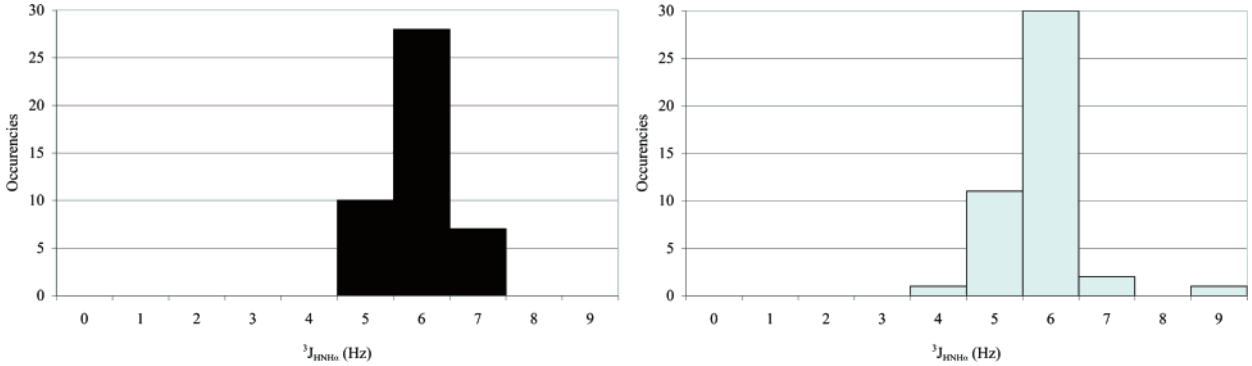

FIGURE 6: Histograms of the homonuclear $^3J_{HNH\alpha}$ coupling constants (in hertz) measured in free Tau (left) and Tau in complex with LMW heparin (right).

importantly, the impossibility to scale both spectra clearly indicates that heparin promotes structural changes. However, without a clear signature of significant secondary structure elements, CD cannot be used to further quantify the secondary structure elements.

The overall structural changes are corroborated by an increased spread of $^3J_{HNH\alpha}$ couplings upon heparin binding. $^3J_{HNH\alpha}$ coupling constants strongly correlate with the backbone Φ angle (*27*), with values of 6−7 Hz indicating fast conformational averaging that characterizes the random coil and values below or above this average indicating α-helical and β-strand propensity, respectively. For 65% of the 44 lysines, we obtained $^3J_{HNH\alpha}$ couplings constants (from 3D HNHA spectra) in the range of 6−7 Hz (Figure 6), consistent with an overall unstructured protein. Upon interaction with the LMW heparin fragment, however, this distribution becomes less homogeneous, with a number of residues showing both smaller and larger coupling constants, suggesting an increase of both α-helical and β-strand content. Finally, although the amide proton chemical shift range does not significantly increase, arguing against a global folding upon interaction with heparin, the 3D NOESY-^{15}N-HSQC spectrum of Tau with a 5-fold excess of LMW heparin showed more H_N-H_N contacts than for free Tau (see below). Together, these data suggest some degree of local structuration induced by heparin binding.

Mapping of the structural changes upon heparin binding. Heparin binding is known to induce α-helical conformation in polylysine peptides (41), and this tendency was also detected for several lysine-rich regions in Tau. Carbon chemical shifts of the Thr149(Lys150) residue within a lysine-rich region, for example, do not change significantly between either free or complexed Tau; yet, the $^3J_{HNH\alpha}$ coupling of Lys150 decreases by 10% from 6.8 to 6.1 Hz upon addition of LMW heparin, suggesting increased helix propensity. Still, within the framework of the full-length protein, a detailed analysis of this fragment leading to a specification of the fractional helix content cannot easily be obtained.

The prominent regions of strong heparin binding cluster in and around the MTBR, with a particularly strong interaction in R1, R2, and R3, but equally in the proline-rich region preceding R1 and the region downstream of R4. We investigated whether the binding results in a similarly increased helix propensity or in other structural changes that might explain the increased tendency of Tau to aggregate when complexed to heparin. Within the MTBR, Val256-(Lys257) in R1 already shows C_α/C_β/CO chemical shifts of 62.6/32.5/176.3 ppm in free Tau at 20 °C, indicating a bias toward local β-strand structure. Within the resolution available from the 3D spectra, these values do not change in the LMW heparin complexed Tau. In R3, the $IVYK_{311}$ motif for free Tau shows C_α/C_β/CO chemical shifts of 57.8/38.9/175.1 ppm for Tyr310 and an H_α shift of 4.56 ppm for Lys311, and virtually unchanged 57.7/38.9/175.03 and 4.55 ppm in the heparin-complexed form. The negative deviations of the C_α and CO shifts from the random coil values hereby support a propensity toward β structure for Tyr310 (*30*) and are supported by the positive H_α deviation for Lys311 (*31*). The $^3J_{HNH\alpha}$ coupling for Lys311 increased by almost 10% from 7.0 to 7.7 Hz in the complexed form, in agreement with an increased propensity of β structure in the Tau/LMW heparin complex. In comparison, the identical $IVYK_{395}$ sequence in the C-terminal domain shows invariant C_α/C_β/CO chemical shifts of 58.0/38.9/175.3 ppm for Tyr394 in both free and heparin complexed Tau. Here, except for the CO shift that might suggest some propensity for β structure if a residue-specific correction factor is applied (*32*), deviations from the random coil values are too small to indicate any propensity for secondary structure, and for Tyr394, the $^3J_{HNH\alpha}$ coupling was unaffected by heparin addition. Comparison of both identical fragments illustrates that heparin binding has a stronger effect upon local secondary structure within R3.

We then analyzed the Glu342-Lys343, Phe346-Lys347 and Asn368-Lys369 pairs within R4. Whereas the carbon chemical shifts for all three residues preceding the Lys do not suggest any residual secondary structure, be it without or with heparin, the $^3J_{HNH\alpha}$ coupling of Lys343 increases from 6.0 Hz (free Tau) to 6.5 Hz (complexed Tau), whereas the $^3J_{HNH\alpha}$ couplings decreases from 6.3 Hz (free Tau) to 5.6 Hz (complexed Tau) for the nearby Lys369, suggesting some helix propensity. The H_α chemical shift of Lys347 (4.19 ppm) does confirm this increased propensity for α-helix in the second part of the R4 repeat. In this same region, we find one of the scarce NOE traces that could tentatively be assigned from the 3D NOESY-HSQC spectrum. Figure 7 shows the 1D NOE trace through the degenerate cross-peak for Gly261 and Gly355, which are both surrounded by an Ile in the $(i - 1)$ and a Ser in the $(i + 1)$ position. Both glycines interact with heparin and experience a concomitant downfield shift by 0.08 ppm in their H^N frequency. In free Tau, both amide protons show NOE contacts to some H_α protons; addition of heparin produces several additional

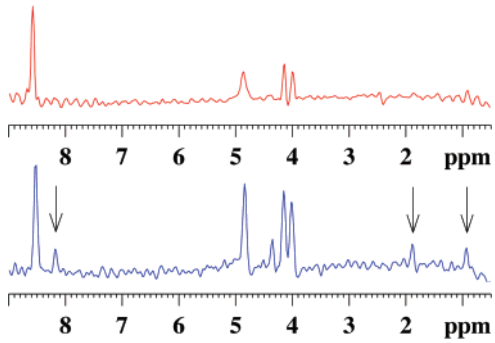

FIGURE 7: Traces through the (Ile)Gly peak from the 3D NOESY-^{15}N-HSQC spectra of isolated Tau (red) or of Tau with a 5-fold excess of LMW heparin.

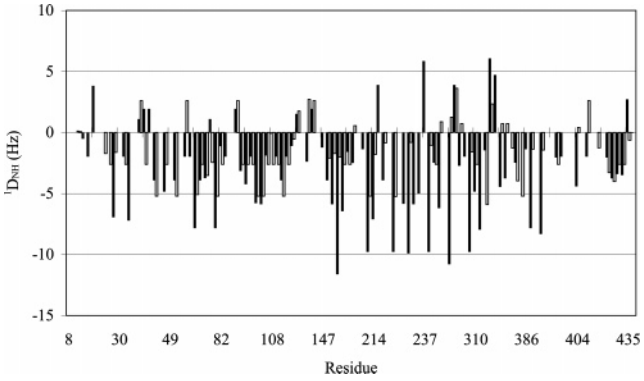

FIGURE 8: Sequential plot of $^1D_{NH}$ residual dipolar couplings (RDCs) (in hertz) extracted from [U-^{15}N]-labeled samples for Tau (black bars) and Tau complexed to LMW heparin (gray bars) measured after alignment with 5% $C_{12}E_5$/hexanol = 0.85 at 20 °C.

contacts, including a novel contact with an amide proton at 8.20 ppm and with some aliphatic protons. Probably, these signals belong to the isoleucine in the (i − 1) position, confirming that the second part of R4 adopt some α-helical structure upon heparin binding. Importantly, although the majority of the H_N-H_N NOE contacts could not be assigned due to severe spectral overlap, the isolated amide signals belonging to residues in R2 and R3 did not show any novel contacts, despite their pronounced interaction with heparin (Figure 4).

RDCs are informative orientational probes (*42*) for residual local structure in otherwise weakly structured polypeptides and folding intermediates (*43*, *44*). Thus, RDCs were measured on [U-^{15}N] samples in order to probe any global structural changes. The constant line widths observed for Tau in the dilute liquid crystalline phase confirmed that the chosen alignment medium does not interact significantly with the unfolded protein and therefore largely retains its isotropic tumbling rate. Moreover, the absence of significant chemical shift differences between spectra recorded in the presence and absence of poly(ethylene glycol) confirmed that this nonionic liquid crystalline medium does not greatly perturb the ensemble of conformations. The nonzero RDC values obtained confirm that Tau can be oriented by this alcohol mixture, and their significant magnitude hints to an extended average shape, in agreement with previous biophysical studies (*5*, *6*). A distinct distribution of negative couplings was observed for Tau (Figure 8), proving that the long axis of this overall random coil polypeptide is aligned with the magnetic field. Tau in complex with short heparin LMW displays generally smaller magnitude RDC values than the free protein. Because this tendency is more pronounced in the Lys-rich region and the MTBR where structural changes occur upon heparin binding (according to chemical shift deviations and $^3J_{HNH\alpha}$ couplings measurements; see above), we interpret these smaller RDC values as the signature of a different orientation of the (local) alignment tensor, rather than of a larger mobility of the polypeptide backbone in the complex. Whether this corresponds to the opening of the global hairpin model (*7*) cannot be concluded at this stage.

Focusing again on the lysine residues, we measured RDC values on the specifically ^{15}N-Lys-labeled sample. As shown in Figure 9, the change in sign of the $^1D_{NH}$ upon heparin binding for Lys298 suggests that the binding of LMW heparin to R2 (the 10 μM K_D value of Lys298 indicates a complete occupancy at this site) does induce the reorientation of this segment with respect to the global alignment tensor, be it due to the change of the latter or to a local structural change. In the other repeats, we equally measured significant changes, with Lys347 in R4 experiencing a change in RDC sign upon LMW heparin. If we correlate this latter sign change with the increase in helix propensity (as shown by $^3J_{HNH\alpha}$ measurements) found in that region upon heparin binding, the helix formation would be coincident with a change in $N-H^N$ orientation for this residue with respect to the global alignment tensor.

DISCUSSION

Although Tau is mostly hyperphosphorylated when integrated into PHF in Alzheimer diseases, little is known about whether and how this posttranslational modification lead to the aggregation of the neuronal microtubule-associated Tau protein. It seems well established that short hexapeptides in the R2 or R3 repeat are involved directly in the PHF formation (*18*, *45*). In comparison with findings on isolated model peptides, we expect their net charge to be of direct influence on their capacity to form amyloid structures (*39*, *40*). Charge compensation in the regions flanking the MTBR as a result of phosphate incorporation has been invoked as another possible factor that can promote aggregation of this otherwise extremely soluble protein (*46*). In this latter study, a hypothetical scheme of the phosphorylation-induced self assembly of wild-type full-length Tau was proposed. Without phosphorylation, both regions N- and C-terminal to the MTBRs fold back onto and protect these repeated fragments from aggregating. Phosphorylation at Ser396 and/or Ser404 would open the segment, allowing Tau−Tau interactions through the repeats. In agreement with this, the isolated MTBR domains (as in the K18 and K19 fragments) indeed aggregate more readily than full-length Tau, suggesting that the other regions play an active solubilizing role, possibly due to their charged nature or conformation. Yet, whether this charge compensation likewise induces structural changes that drive the protein toward a cross-β structure, as commonly assumed for the core region of the PHF (*47*, *48*), clearly requires structural studies on the full-length protein, which is the aim of the present work.

Because of the difficulties associated with quantification and reproducibility of *in vitro* phosphorylation (*49*), the finding that polyanions can cause Tau aggregation without this posttranslational modification has opened a way for

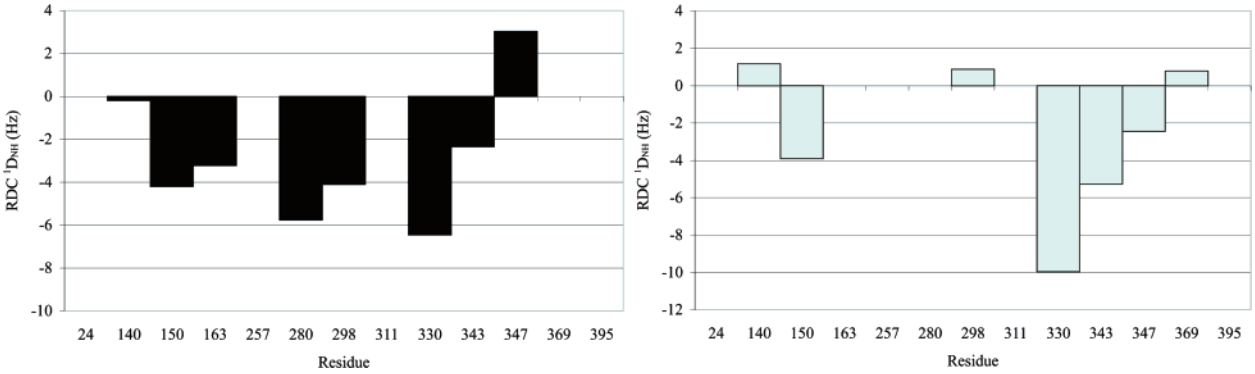

FIGURE 9: Sequential plot of $^1D_{NH}$ residual dipolar couplings (RDCs) (in hertz) for assigned lysine residues extracted from [U-^{13}C,Lys-^{15}N]-labeled samples for Tau (left) and Tau in complex with unlabeled short heparin (right) measured after alignment with 5% $C_{12}E_5$/hexanol = 0.85 at 20 °C.

further studies on the aggregation process (*14*−*17*, *50*). Heparin or other sulfated glycosaminoglycans (GAGs) are of considerable interest as a causative agent for Tau aggregation (*51*), but here again, little is known about the molecular details of this interaction. The technical difficulties in characterizing the complex originate in both components. Tau is a largely unstructured polypeptide, as determined by macroscopic techniques, e.g., CD, SAXS, or IR (*5*, *6*), and heparin, when isolated from a natural source, is invariably a heterogeneous mixture with a distribution of molecular sizes and sulfation patterns (*19*). The most highly sulfated regions of heparin, however, have an unusually well-defined solution conformation for a linear polysaccharide (*52*). Unlike most polysaccharides, they adopt a relatively stiff, well-defined linear structure rather than random coil, and tend to induce α-helical structure in basic peptides such as polylysine (*41*), which might be a well-suited model for the Tau protein with its many basic residues. Remarkably, both a minimal length and charge density seem to be required for inducing aggregation of Tau into PHF (*14*, *53*), in agreement with recent findings on the acceleration of amyloid formation of gelsolin by heparin (*38*).

In our study, we have used full-length Tau and two different heparin polymers in order to evaluate the structural impact of polyanion binding. HMW heparin is able to induce aggregation when incubated at substoichiometric ratios at 37 °C but the aggregation at room temperature is very slow (*37*) on the time scale of the recording for a NMR ^{15}N-HSQC spectra. NMR with these samples thus mainly observes binding rather than aggregation, with chemical shift differences monitoring the sole binding event. Upon titration of the heparin, we observed in this manner binding of the polyanion to both MTBR flanking regions, with important changes in the proline-rich region (see Ala227 and Ala246 in Figure 3A) and in the lysine-rich region downstream of the fourth repeat (with three lysines at positions 375, 383, and 385). Significant changes were also observed for resonances of residues within the MTBR. The line broadening of most resonances upon interaction with this HMW heparin, however, hinders further characterization of the complex and of induced structural changes. Because this line broadening probably results from the simultaneous interaction of several negatively charged heparin building blocks with different anchoring points on the protein, we switched our experimental system to a shorter and better characterized 4.2 kDa heparin fragment, containing 14 disaccharide units (LMW heparin). The binding of this fragment is very similar, as indicated by similar chemical shift changes observed in the titration experiments (compare Figure 3A and Figure 3F). Nonetheless, as expected, the smaller size of this heparin induces less line broadening probably due to faster exchange kinetics on the NMR time scale. The gradual shift of Tau signals upon heparin addition thereby allowed us to rank the different regions according to their binding strength. Fitting of the corresponding titration curves to a one site/one ligand model (Figure 4) offered a more quantitative view on heparin binding to Tau, with several high-affinity binding sites clustering in the MTBR, in the proline-rich region, and in the region immediately downstream of the MTBR. The observation of tight binding to A227 (Figure 3A and G), V229, and R230 supports the hypothesis that the introduction of negative charges in this region might decrease the solubilizing effect of this region, and the same conclusion is valid for the region downstream of the R4 repeat. Phosphorylation of Thr212/Ser214 or Thr231/Ser235, two of the abnormal phosphorylation patterns characterizing Tau aggregated into PHF (*54*), or alternatively of Ser396/Ser404, two other phosphorylation sites that characterize PHF-Tau (*46*), therefore might indeed be a causative event leading to aggregation.

Besides the questions of where and how strongly heparin interacts with Tau, we investigated the structural consequences of this molecular interaction. Our findings on the structural changes induced by heparin binding can be summarized as follows.

(1) α*-Helical Structure in the Presence of Heparin for Those Regions That Resemble Polylysine*. The only region where heparin binding is in the slow exchange regime on the NMR time scale, characterized by the coexistence of resonances of the free and complexed Tau Ala152 (Figure 3), is the D_{149}KKAKG_{154} fragment downstream of the two N-terminal inserts encoded by exons 2 and 3 (*1*). The strongly negatively charged heparin prefers the positively charged lysine and arginine residues as principal binding motif (*19*), where it can induce helix formation (*41*). The reduction of RDCs in this region (Figure 8) could be due either to a larger mobility of the complex averaging the values or to a different orientation of $N-H^N$ vectors within induced α-helical structures with their long axes parallel to the magnetic field. However, we find a 0.6 Hz reduction in the $^3J_{HNH\alpha}$ of Lys150, consistent with an increased helix propensity in the Tau/LMW heparin complex.

Thus, RDCs would be better attributed to orientational changes due to helix propensity increase. The regular periodicity of sulfate group clusters in heparin was found to match with a periodicity of eleven residues (i.e., three turns) on the polylysine peptide α-helix (*37*). Remarkably, the same periodicity of 11 residues could be found for two consecutive lysines within this lysine-rich regions of Tau (K_{130}SKDGTGSDDK$_{140}$K$_{141}$AKGADGKTK$_{150}$), whereby the lysine side chains hence could project in a similar manner toward a group of sulfates on the heparin.

(2) V_{306}QIVYK$_{311}$ (PHF6) Has a Propensity for β Structure That Is Even Reinforced after Adding Heparin. A second zone of strong interaction lies in the second (R2 residues 274−304) and third (R3 residues 305−335) microtubule binding repeats, with measured K_D values in the range of 10 μM. A previous NMR study on the R3 or R4 repeat domains of fetal or adult Tau equally defined these interaction zones on the basis of important chemical shifts induced by the binding of an even shorter heparin fragment (*9*). An increase in β-sheet population upon interaction with a heparin fragment could promote fiber formation, although previous studies failed to detect a correlation between the propensity of β-sheet structure in Tau and its aggregation (*55*). The analysis of chemical shift deviations from random coil values, sensitive to backbone conformation (*30*), suggests more residual local β structure for the central IVYK$_{311}$ than for the C-terminal IVYK$_{396}$ motif. Interestingly, the former motif is part of the so-called PHF6 sequence V$_{306}$QIVYK$_{311}$ known to be a potential nucleation site for the aggregation of Tau in PHF (*18*). Moreover, this indicated residual β structure is enhanced by the addition of heparin, as suggested by an increase of 0.6 Hz in the $^3J_{HNHα}$ coupling constant of Lys$_{311}$. These findings confirm that a preexisting β structure (rather than a specific sequence) could be the recognition motif for the aggregation initiation, since the same sequence also exists at the C-terminus of full-length Tau, but is not involved in its aggregation into PHF.

(3) Repeat R4 of the MTBR Has Residual Helix Propensity. The beginning of repeat R4 (residues 336−367) seems to be less sensitive to helical formation relative to its end. From the Hα secondary shifts and the smaller $^3J_{HNHα}$ couplings, however, it seems that the second part of repeat R4 has some residual helix structure, and here again, we find the 11-residue spacing that characterizes the polylysine/heparin complex (K$_{343}$KDFKDRVQSK$_{353}$). After heparin addition, the 3D NOESY-^{15}N-HSQC spectrum reveals several new NOE contacts for a degenerate (Ile)Gly motif that could belong to either position 261 or position 355 (Figure 7). In combination with the smaller coupling constants observed in this region, it seems plausible that these NOE contacts belong to Gly355 and might correspond to the characteristic (i, i + 1) H_N-H_N NOE between amide protons of residues within an α-helix. Interestingly, a change in RDC sign of Lys347 in R4 (Figure 9) accompanies this increased α-helical content, as in the lysine-rich region discussed above. Increased helical propensity upon LWM heparin binding hence seems accompanied by a differential orientation of the $N-H^N$ vectors with respect to the overall alignment tensor.

Our data indicating the induction of both α-helical and extended β structure in different parts of the protein (Figure 10) shed further light on the recent debate on the secondary

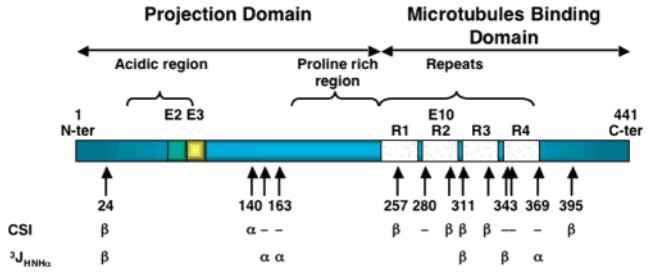

FIGURE 10: Domain structure of Tau and chemical shift index (CSI) consensus converted in secondary structure (α helix, β shift, or − random coil). In front of $^3J_{HNHα}$ is represented the tendency of secondary structure increases from free Tau to Tau complexed to heparin.

structure elements of PHF-Tau. IR and CD spectroscopy, indeed, provide evidence for α-helical conformation in PHF isolated from brains of Alzheimer's diseased patients (*56*, *57*), although those data were immediately challenged by X-ray and electron diffraction data on both *in vitro* and *in vivo* generated PHF (*47*, *48*). Renewed support for nascent α-helical conformation came NMR chemical shift values obtained at low temperature on the isolated three repeat (R1, R3, and R4) K19 fragment, suggesting the presence of α-helical propensity even in repeats R1 and R4 (*8*). Again, however, a second low-temperature NMR study on the isolated three or four repeat regions derived from fetal Tau352 or adult Tau441 (*9*) failed to confirm the presence of this α-helical structure. Our present structural data on the full-length protein give a more mixed picture, whereby heparin binding does more than just provide a network of negative charges, but enforces different structural tendencies depending on where the interaction takes place. Chemical shift deviations, $^3J_{HNHα}$ couplings, RDCs, and NOE data on the full-length protein indicate that the heparin polyanion induces some α-helical conformation but not necessarily in the regions that form the core of the PHF (Figure 7). The IR and CD spectroscopic evidence on the native PHF (*57*) might therefore well come from those parts of Tau complexed to a sulfated glycosaminoglycan or other polyanion but not rigidly integrated in the core of the PHF, thereby escaping detection by diffraction techniques that require the presence of an ordered lattice. Those latter electron or X-ray diffraction techniques would only observe the rigid parts of the PHF core, characterized by the cross-β structure. The extended β structure that this requires for the polypeptide backbone, already present in certain fragments of the MTBR, is further enforced by complexation of the polyanion. Here, we cannot confirm whether hyperphosphorylation, beyond its influence on the charge state of the regions directly flanking the MTBRs (*46*), has similar structural consequences on the MTBRs themselves and hence contributes in a similar way to the aggregation mechanism as heparin, but it would be an additional argument to link this posttranslational modification to the aggregation behavior of Tau.

While our results support the hypothesis that heparin interaction both with peptides in R2/R3 and with the basic regions flanking the MTBR, through structural changes in the former and charge neutralization followed by an overall structural change in the latter, enables aggregation of Tau into PHF, it is unclear how heparin integrates into the fibers. Our NMR observation that predominant interaction sites for heparin such as the region around Ala152 and the proline-

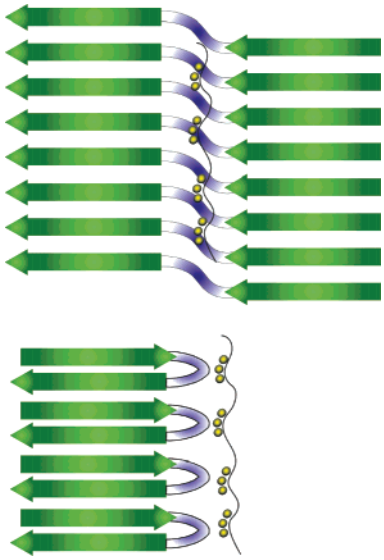

FIGURE 11: Working model of integration of heparin into the PHF. Green arrows represent the amyloid peptides in the repeats R2 and R3, separated by the basic lysines (blue) located in the central part of each repeat. The sulfate moieties of heparin are represented in yellow. The parallel, in-register alignment of the hydrophobic peptides within R2 and R3 exposes a continuous polylysine surface that sequesters the heparin into the core of the PHF.

rich region around Thr231 are no longer in interaction with the glycosaminoglycan when Tau becomes integrated in the PHFs strongly suggests that all heparin is integrated in the rigid core and therefore escapes detection by solution NMR methods. Beyond the cross-β structure revealed by fiber diffraction experiments, little is known about the atomic details of this rigid core region. EPR data on full-length Tau PHF suggest parallel β-sheets in register (*58*), similar to the recently obtained high-resolution data on amyloid fibers of prion (*59*, *60*) or β-amyloid peptides (*61*). Those peptide fibrils show a "dry" interface where the shape complementarity of facing side chains leaves little room even for water molecules (*59*), further excluding the possibility that heparin intercalates between the facing β-sheets. The peptides, however, are rather small, and if we consider the R2 and R3 repeats, we can imagine that they would be no longer than the V_{275}QIINK$_{280}$ (in PHF6*) or V_{306}QIVYK$_{311}$ (in PHF6) hexapeptides. Stacking of these peptides in parallel in register β-sheets would, however, lead to the same stacking of the following residues, which are a Lys-Lys and a Lys-Pro motif, respectively. This would create a continuous stretch of positive charges with accompanying strong electrostatic repulsion, unless a mechanism of charge neutralization is provided. One of such mechanisms is the deletion of at least one lysine, and ΔK$_{280}$ indeed is a mutant which aggregates more rapidly (*62*). The present study suggests a model where the heparin polymer wraps tightly around the outer surface of the (double) pleated sheets and thereby neutralizes the inhibitory charge repulsions that would occur in a continuous but intermolecularly formed polylysine stretch (Figure 11).

In conclusion, our titration experiments with different heparin fragments have revealed zones of strong to intermediate binding that correspond to the region immediately following the two inserts encoded by exons 2 and 3, to residues in the repeats R2 and R3, and to two regions N- and C-terminal of the MTBR. Charge neutralization as a result of binding to the two regions up- and downstream of the MTBR, which were proposed to inhibit the aggregation process, well mimicks the hyperphosphorylation that characterizes *in vivo* generated PHF-Tau. Our investigation on the structural impact of heparin binding to full-length Tau by NMR spectroscopy reveals increased residual β-sheet propensity within peptides of the R2 and R3 repeat upon binding of heparin, which probably is a prerequisite for Tau aggregation into PHF. Both the polylysine sequence in the N-terminal part of Tau and the second half of the R4 repeat of the MTBR tend to form a helical structure in the presence of heparin. Upon formation of the PHF, all heparin-induced chemical shift differences tend to disappear. We propose that parallel, in-register alignment of the hydrophobic peptides within R2 and R3 exposes a continuous polylysine surface. High-affinity binding of heparin during the PHF growth provides the necessary charge compensation to allow the fiber growth and explains why we do not find any heparin-induced chemical shifts in the flexible parts of Tau after integration into the fibrils.

SUPPORTING INFORMATION AVAILABLE

Table S1 showing the $^3J_{HNH\alpha}$ couplings (in hertz) derived from 3D HNHA experiments for free Tau in solution and complexed Tau to heparin (LMW). This material is available free of charge via the Internet at http://pubs.acs.org.

REFERENCES

1. Buee, L., Bussiere, T., Buee-Scherrer, V., Delacourte, A., and Hof, P. R. (2000) Tau protein isoforms, phosphorylation and role in neurodegenerative disorders, *Brain Res. Brain Res. Rev. 33*, 95−130.
2. Delacourte, A., and Defossez, A. (1986) Alzheimer's disease: Tau proteins, the promoting factors of microtubule assembly, are major components of paired helical filaments, *J. Neurol. Sci. 76*, 173−186.
3. Grundke-Iqbal, I., Iqbal, K., Quinlan, M., Tung, Y. C., Zaidi, M. S., and Wisniewski, H. M. (1986) Microtubule-associated protein tau. A component of Alzheimer paired helical filaments, *J. Biol. Chem. 261*, 6084−6089.
4. Bennett, D. A., Schneider, J. A., Wilson, R. S., Bienias, J. L., and Arnold, S. E. (2004) Neurofibrillary tangles mediate the association of amyloid load with clinical Alzheimer disease and level of cognitive function, *Arch. Neurol. 61*, 378−384.
5. Cleveland, D. W., Hwo, S. Y., and Kirschner, M. W. (1977) Physical and chemical properties of purified tau factor and the role of tau in microtubule assembly, *J. Mol. Biol. 116*, 227−247.
6. Schweers, O., Schonbrunn-Hanebeck, E., Marx, A., and Mandelkow, E. (1994) Structural studies of tau protein and Alzheimer paired helical filaments show no evidence for beta-structure, *J. Biol. Chem. 269*, 24290−24297.
7. Jeganathan, S., von Bergen, M., Brutlach, H., Steinhoff, H. J., and Mandelkow, E. (2006) Global hairpin folding of tau in solution, *Biochemistry 45*, 2283−2293.
8. Eliezer, D., Barre, P., Kobaslija, M., Chan, D., Li, X., and Heend, L. (2005) Residual structure in the repeat domain of tau: echoes of microtubule binding and paired helical filament formation, *Biochemistry 44*, 1026−1036.
9. Mukrasch, M. D., Biernat, J., von Bergen, M., Griesinger, C., Mandelkow, E., and Zweckstetter, M. (2005) Sites of tau important for aggregation populate {beta}-structure and bind to microtubules and polyanions, *J. Biol. Chem. 280*, 24978−24986.
10. Lippens, G., Wieruszeski, J. M., Leroy, A., Smet, C., Sillen, A., Buee, L., and Landrieu, I. (2004) Proline-directed random-coil chemical shift values as a tool for the NMR assignment of the tau phosphorylation sites, *ChemBioChem 5*, 73−78.
11. Lippens, G., Sillen, A., Smet, C., Wieruszeski, J. M., Leroy, A., Buee, L., and Landrieu, I. (2006) Studying the natively unfolded neuronal Tau protein by solution NMR spectroscopy, *Protein Pept. Lett. 13*, 235−246.

12. Biernat, J., Gustke, N., Drewes, G., Mandelkow, E. M., and Mandelkow, E. (1993) Phosphorylation of Ser262 strongly reduces binding of tau to microtubules: distinction between PHF-like immunoreactivity and microtubule binding, *Neuron 11*, 153−163.
13. Hasegawa, M., Morishima-Kawashima, M., Takio, K., Suzuki, M., Titani, K., and Ihara, Y. (1992) Protein sequence and mass spectrometric analyses of tau in the Alzheimer's disease brain, *J. Biol. Chem. 267*, 17047−17054.
14. Goedert, M., Jakes, R., Spillantini, M. G., Hasegawa, M., Smith, M. J., and Crowther, R. A. (1996) Assembly of microtubule-associated protein tau into Alzheimer-like filaments induced by sulphated glycosaminoglycans, *Nature 383*, 550−553.
15. Hasegawa, M., Crowther, R. A., Jakes, R., and Goedert, M. (1997) Alzheimer-like changes in microtubule-associated protein Tau induced by sulfated glycosaminoglycans. Inhibition of microtubule binding, stimulation of phosphorylation, and filament assembly depend on the degree of sulfation, *J. Biol. Chem. 272*, 33118−33124.
16. Kampers, T., Friedhoff, P., Biernat, J., Mandelkow, E. M., and Mandelkow, E. (1996) RNA stimulates aggregation of microtubule-associated protein tau into Alzheimer-like paired helical filaments, *FEBS Lett. 399*, 344−349.
17. Wilson, D. M., and Binder, L. I. (1997) Free fatty acids stimulate the polymerization of tau and amyloid beta peptides. In vitro evidence for a common effector of pathogenesis in Alzheimer's disease, *Am. J. Pathol. 150*, 2181−2195.
18. von Bergen, M., Friedhoff, P., Biernat, J., Heberle, J., Mandelkow, E. M., and Mandelkow, E. (2000) Assembly of tau protein into Alzheimer paired helical filaments depends on a local sequence motif ((306)VQIVYK(311)) forming beta structure, *Proc. Natl. Acad. Sci. U.S.A. 97*, 5129−5134.
19. Capila, I., and Linhardt, R. J. (2002) Heparin-protein interactions, *Angew. Chem., Int. Ed. Engl. 41*, 391−412.
20. Sachchidanand, Lequin, O., Staunton, D., Mulloy, B., Forster, M. J., Yoshida, K., and Campbell, I. D. (2002) Mapping the heparin-binding site on the 13-14F3 fragment of fibronectin, *J. Biol. Chem. 277*, 50629−50635.
21. Mulloy, B., Forster, M. J., Jones, C., and Davies, D. B. (1993) N.m.r. and molecular-modelling studies of the solution conformation of heparin, *Biochem. J. 293* (Part 3), 849−858.
22. Ruckert, M., and Otting, G. (2000) Alignment of biological macromolecules in novel nonionic liquid crystalline media for NMR experiments, *J. Am. Chem. Soc. 122*, 7793−7797.
23. Mach, H., Middaugh, C. R., and Lewis, R. V. (1992) Statistical determination of the average values of the extinction coefficients of tryptophan and tyrosine in native proteins, *Anal. Biochem 200*, 74−80.
24. Palmer, A. G., Cavanagh, J., Wright, P. E., and Rance, M. (1991) Sensitivity improvement in proton-detected 2-dimensional heteronuclear correlation NMR-spectroscopy, *J. Magn. Reson. 93*, 151−170.
25. Grzesiek, S., and Bax, A. (1993) Amino acid type determination in the sequential assignment procedure of uniformly 13C/15N-enriched proteins, *J. Biomol. NMR 3*, 185−204.
26. Grzesiek, S., and Bax, A. (1992) Improved 3d triple-resonance NMR techniques applied to a 31-kda protein, *J. Magn. Reson. 96*, 432−440.
27. Vuister, G. W., and Bax, A. (1993) Quantitative J correlation−A new approach for measuring homonuclear 3-bond J(H(N)H(alpha) coupling-constants in N-15-enriched proteins, *J. Am. Chem. Soc. 115*, 7772−7777.
28. Grzesiek, S., and Bax, A. (1993) The importance of not saturating H_2O in protein NMR−Application to sensitivity enhancement and NOE measurements, *J. Am. Chem. Soc. 115*, 12593−12594.
29. Cordier, F., Dingley, A. J., and Grzesiek, S. (1999) A doublet-separated sensitivity-enhanced HSQC for the determination of scalar and dipolar one-bond J-couplings, *J. Biomol. NMR 13*, 175−180.
30. Wishart, D. S., and Sykes, B. D. (1994) The 13C chemical-shift index: a simple method for the identification of protein secondary structure using 13C chemical-shift data, *J. Biomol. NMR 4*, 171−180.
31. Wishart, D. S., Sykes, B. D., and Richards, F. M. (1992) The chemical shift index: a fast and simple method for the assignment of protein secondary structure through NMR spectroscopy, *Biochemistry 31*, 1647−1651.
32. Schwarzinger, S., Kroon, G. J., Foss, T. R., Chung, J., Wright, P. E., and Dyson, H. J. (2001) Sequence-dependent correction of random coil NMR chemical shifts, *J. Am. Chem. Soc. 123*, 2970−2978.
33. Kay, L. E., Torchia, D. A., and Bax, A. (1989) Backbone dynamics of proteins as studied by 15N inverse detected heteronuclear NMR spectroscopy: application to staphylococcal nuclease, *Biochemistry 28*, 8972−8979.
34. Baleja, J. D., Mau, T., and Wagner, G. (1994) Recognition of DNA by GAL4 in solution: use of a monomeric protein-DNA complex for study by NMR, *Biochemistry 33*, 3071−3078.
35. Mulloy, B., Gray, E., and Barrowcliffe, T. W. (2000) Characterization of unfractionated heparin: comparison of materials from the last 50 years, *Thromb. Haemostasis 84*, 1052−1056.
36. Sillen, A., Leroy, A., Wieruszeski, J. M., Loyens, A., Beauvillain, J. C., Buee, L., Landrieu, I., and Lippens, G. (2005) Regions of tau implicated in the paired helical fragment core as defined by NMR, *ChemBioChem 6*, 1849−1856.
37. Friedhoff, P., Schneider, A., Mandelkow, E. M., and Mandelkow, E. (1998) Rapid assembly of Alzheimer-like paired helical filaments from microtubule-associated protein tau monitored by fluorescence in solution, *Biochemistry 37*, 10223−10230.
38. Suk, J. Y., Zhang, F., Balch, W. E., Linhardt, R. J., and Kelly, J. W. (2006) Heparin accelerates gelsolin amyloidogenesis, *Biochemistry 45*, 2234−2242.
39. Lopez De La Paz, M., Goldie, K., Zurdo, J., Lacroix, E., Dobson, C. M., Hoenger, A., and Serrano, L. (2002) De novo designed peptide-based amyloid fibrils, *Proc. Natl. Acad. Sci. U.S.A. 99*, 16052−16057.
40. Inouye, H., Sharma, D., Goux, W. J., and Kirschner, D. A. (2006) Structure of core domain of fibril-forming PHF/Tau fragments, *Biophys. J. 90*, 1774−1789.
41. Mulloy, B., Crane, D. T., Drake, A. F., and Davies, D. B. (1996) The interaction between heparin and polylysine: a circular dichroism and molecular modelling study, *Braz. J. Med. Biol. Res. 29*, 721−729.
42. Tjandra, N., and Bax, A. (1997) Direct measurement of distances and angles in biomolecules by NMR in a dilute liquid crystalline medium, *Science 278*, 1111−1114.
43. Shortle, D., and Ackerman, M. S. (2001) Persistence of native-like topology in a denatured protein in 8 M urea, *Science 293*, 487−489.
44. Louhivuori, M., Paakkonen, K., Fredriksson, K., Permi, P., Lounila, J., and Annila, A. (2003) On the origin of residual dipolar couplings from denatured proteins, *J. Am. Chem. Soc. 125*, 15647−15650.
45. Barghorn, S., Zheng-Fischhofer, Q., Ackmann, M., Biernat, J., von Bergen, M., Mandelkow, E. M., and Mandelkow, E. (2000) Structure, microtubule interactions, and paired helical filament aggregation by tau mutants of frontotemporal dementias, *Biochemistry 39*, 11714−11721.
46. Alonso, A., Mederlyova, A.., Novak, M., Grundke-Iqbal, I., and Iqbal, K. (2004) Promotion of hyperphosphorylation by Frontotemporal dementia Tau mutations, *J. Biol. Chem. 279*, 34873−34881.
47. Barghorn, S., Davies, P., and Mandelkow, E. (2004) Tau paired helical filaments from Alzheimer's disease brain and assembled in vitro are based on beta-structure in the core domain, *Biochemistry 43*, 1694−1703.
48. Berriman, J., Serpell, L. C., Oberg, K. A., Fink, A. L., Goedert, M., and Crowther, R. A. (2003) Tau filaments from human brain and from in vitro assembly of recombinant protein show cross-beta structure, *Proc. Natl. Acad. Sci. U.S.A. 100*, 9034−9038.
49. Landrieu, I., Lacosse, L., Leroy, A., Wieruszeski, J. M., Trivelli, X., Sillen, A., Sibille, N., Schwalbe, H., Saxena, K., Langer, T., and Lippens, G. (2006) NMR analysis of a Tau phosphorylation pattern, *J. Am. Chem. Soc. 128*, 3575−3583.
50. Perez, M., Valpuesta, J. M., Medina, M., Montejo de Garcini, E., and Avila, J. (1996) Polymerization of tau into filaments in the presence of heparin: the minimal sequence required for tau-tau interaction, *J. Neurochem. 67*, 1183−1190.
51. Perry, G., Siedlak, S. L., Richey, P., Kawai, M., Cras, P., Kalaria, R. N., Galloway, P. G., Scardina, J. M., Cordell, B., Greenberg, B. D., et al. (1991) Association of heparan sulfate proteoglycan with the neurofibrillary tangles of Alzheimer's disease, *J. Neurosci. 11*, 3679−3683.
52. Mulloy, B., Gee, C., Wheeler, S. F., Wait, R., Gray, E., and Barrowcliffe, T. W. (1997) Molecular weight measurements of

low molecular weight heparins by gel permeation chromatography, *Thromb. Haemostasis 77*, 668−674.
53. Arrasate, M., Perez, M., Valpuesta, J. M., and Avila, J. (1997) Role of glycosaminoglycans in determining the helicity of paired helical filaments, *Am. J. Pathol. 151*, 1115−1122.
54. Hoffmann, R., Lee, V. M., Leight, S., Varga, I., and Otvos, L., Jr. (1997) Unique Alzheimer's disease paired helical filament specific epitopes involve double phosphorylation at specific sites, *Biochemistry 36*, 8114−8124.
55. Ruben, G. C., Ciardelli, T. L., Grundke-Iqbal, I., and Iqbal, K. (1997) Alzheimer disease hyperphosphorylated tau aggregates hydrophobically, *Synapse 27*, 208−229.
56. Kunjithapatham, R., Oliva, F. Y., Doshi, U., Perez, M., Avila, J., and Munoz, V. (2005) Role for the alpha-helix in aberrant protein aggregation, *Biochemistry 44*, 149−156.
57. Sadqi, M., Hernandez, F., Pan, U., Perez, M., Schaeberle, M. D., Avila, J., and Munoz, V. (2002) Alpha-helix structure in Alzheimer's disease aggregates of tau-protein, *Biochemistry 41*, 7150−7155.
58. Margittai, M., and Langen, R. (2004) Template-assisted filament growth by parallel stacking of tau, *Proc. Natl. Acad. Sci. U.S.A. 101*, 10278−10283.
59. Nelson, R., Sawaya, M. R., Balbirnie, M., Madsen, A. O., Riekel, C., Grothe, R., and Eisenberg, D. (2005) Structure of the cross-beta spine of amyloid-like fibrils, *Nature 435*, 773−778.
60. Ritter, C., Maddelein, M. L., Siemer, A. B., Luhrs, T., Ernst, M., Meier, B. H., Saupe, S. J., and Riek, R. (2005) Correlation of structural elements and infectivity of the HET-s prion, *Nature 435*, 844−848.
61. Tycko, R. (2004) Progress towards a molecular-level structural understanding of amyloid fibrils, *Curr. Opin. Struct. Biol. 14*, 96−103.
62. Goedert, M., Jakes, R., and Crowther, R. A. (1999) Effects of frontotemporal dementia FTDP-17 mutations on heparin-induced assembly of tau filaments, *FEBS Lett. 450*, 306−311.

BI060964O